THE JOURNAL OF COMPARATIVE NEUROLOGY 408:204–219 (1999)

The Eta Ganglion Cell Type of Cat Retina

D.M. BERSON,* T. ISAYAMA, AND M. PU
Department of Neuroscience, Brown University, Providence, Rhode Island 02912

ABSTRACT

We define a morphologic type of ganglion cell in cat retina by using intracellular staining in vitro. The eta cell has a small soma, slender axon, and delicate, highly branched dendritic arbor. Dendritic fields are intermediate in size among cat ganglion cells, with diameters typically two to three times those of beta cells. Fields increase in size as a function of distance from the area centralis, ranging in diameter from 90 μm to 200 μm centrally to a maximum of 600 μm in the periphery. This increase is unusually radially symmetric. By contrast with other cat ganglion cell types, eta cells do not have markedly smaller dendritic fields within the visual streak than above or below it nor much smaller fields nasally than temporally. Dendrites ramify broadly throughout sublamina *a* (OFF sublayer) of the inner plexiform layer. They arborize most densely in S2, where they costratify with dendrites of OFF alpha cells. There is apparently no matching ON variety of eta cell. Experiments combining retrograde labeling with intracellular staining indicate that eta cells project to the superior colliculus and to two components of the dorsal lateral geniculate nucleus (the C laminae and medial interlaminar nucleus). Eta cells apparently project contralaterally from the nasal retina and ipsilaterally from the temporal retina. The morphology and projection patterns of the eta cell suggest that its physiologic counterpart is a type of sluggish or W-cell with an OFF center, an ON surround, and possibly a transient light response. J. Comp. Neurol. 408:204–219, 1999.

Indexing terms: W-cell; sluggish; visual streak; superior colliculus; lateral geniculate nucleus; medial interlaminar nucleus

The visual scene is analyzed in parallel by many distinct types of retinal ganglion cells. Each type can be viewed as an array of local neural filters that is distributed widely across the retina and exhibits a characteristic tuning to the spatial and temporal structure of the retinal image. The ganglion cell population thus embodies multiple representations of the visual world, each distinct from but spatially interleaved with the others. A comprehensive understanding of this functional design for any retina requires a catalog of its ganglion cell types. Developing such a catalog is not trivial. Ideally, each new type is defined by the covariation of its members on many independent dimensions and is distinguished from other types by the absence of intermediate forms (Boycott and Wässle, 1974; Rowe and Stone, 1977; Rodieck and Brening, 1983; Stone, 1983; Rodieck, 1998).

This ideal has been approached for a handful of morphologic types in several of the best studied mammalian retinas, typically by correlating measures of soma size, dendritic field size, topographic location, and dendritic stratification (see, e.g., Boycott and Wässle, 1974; Dacey, 1989, 1993a,b; Watanabe and Rodieck, 1989; Peichl, 1991; Rodieck and Watanabe, 1993; Vaney, 1994; Pu et al., 1994; Berson et al.,1998). Morphologic diversity among the other ganglion cells in these retinas suggests that many more types remain to be discovered, but formal classification has been hampered by the small number of cells observed and the limited morphometric data obtained from them.

In the cat retina, seven ganglion cell types can be said to have been classified formally by using the above criteria: alpha-ON, alpha-OFF, beta-ON, beta-OFF, delta (monoamine-accumulating), epsilon, and zeta (Boycott and Wässle, 1974; Wässle et al., 1975, 1981; Leventhal et al., 1980; Pu et al., 1994; Dacey, 1989; Wässle and Boycott, 1991; Berson et al., 1998). A wide variety of other forms has been documented and, in some cases, provisionally typed (Boycott and Wässle, 1974; Kolb et al., 1981; Stanford, 1987; Famiglietti, 1987; Berson et al., 1997; Isayama et al., 1997). The present study is a continuation of our ongoing effort to develop a comprehensive morphologic

Grant sponsor: National Eye Institute; Grant number: PHS 5 R01 EY06108.

M. Pu's current address is Department of Neurobiology and Anatomy, University of Utah College of Medicine, Salt Lake City, UT 84132.

*Correspondence to: David M. Berson, Department of Neuroscience, Box 1953, Brown University, Providence, RI 02912.
E-mail: david_berson@brown.edu

Received 14 August 1998; Revised 23 December 1998; Accepted 7 January 1999

typology for these incompletely classified ganglion cells. We have used intracellular staining and retrograde labeling to define a new morphologic type, which we designate the "eta cell," extending the Greek alphabetic series introduced for morphologic types of cat ganglion cells by Boycott and Wässle (1974).

MATERIALS AND METHODS

The methods that were employed in this study are summarized only briefly here, because they have been described in detail previously (Pu and Berson, 1992; Pu et al., 1994; Berson et al., 1998). Unless otherwise noted we use the term "delta" to refer to the morphologic type known to accumulate monoamines (Wässle et al., 1987; Dacey, 1989).

Dye injection and histochemistry

Ganglion cells were stained by visually guided intracellular injection of Lucifer Yellow and either biocytin or Neurobiotin in the living retina in vitro. Methods were approved by Brown University's Institutional Animal Care and Use Committee and conformed with National Institutes of Health guidelines. Cats were deeply anesthetized with Nembutal (35 mg/kg, i.p.) and, following eye removal, killed by Nembutal overdose with or without vascular perfusion with 4% buffered paraformaldehyde, pH 7.4. Retinas were isolated and superfused at room temperature with oxygenated Ames medium (Sigma, St. Louis, MO).

In some experiments (30 retinas from 21 cats), we targeted ganglion cells stained supravitally with acridine orange (for details, see Pu et al., 1994). For the analysis of dendritic stratification, we sometimes impaled and stained one or more marker or fiducial cells (typically alpha cells) in the vicinity of filled eta cells. In other experiments (32 retinas from 19 cats), we injected cells tagged by retrograde transport of fluorescent microspheres deposited in the superior colliculus or lateral geniculate nucleus, as described elsewhere (Pu and Berson, 1991, 1992; Pu et al., 1994; Stein et al., 1996; Berson et al., 1998). Collicular injections were unilateral, spanned all of the superficial layers, and were confined to the colliculus. Except for one deposit, which spread rostrally into the representation of the ipsilateral visual field, they were restricted to the contralateral field representation. Deposits in the medial interlaminar nucleus of the lateral geniculate body were unilateral and spared the A and C layers of the geniculate. They may have involved the geniculate wing in some cases, but this largely can be ignored, because deposits confined to the wing do not label eta cells (Pu et al., 1994). Deposits in the C layers of the lateral geniculate were bilateral and centered in laminae C and C1. Because we sought to avoid involvement of underlying optic fibers, they involved only minimally layers C2 and C3. The medial interlaminar nucleus, geniculate wing, and ventral lateral geniculate nucleus were spared. In most cases, there was some involvement of the overlying A laminae, but these are known to receive input exclusively from alpha and beta ganglion cells (Stone, 1983; Stein et al., 1996).

Alpha, beta, delta, epsilon, and zeta cells stained in these experiments were used for various morphometric comparisons. Table 1 summarizes the types and numbers of ganglion cells recovered in all retinas containing at least one stained eta cell. Comparisons of soma size are based on a sample of 154 zeta cells (mean ± S.D. soma size: 16.0 μm ± 1.7 μm; Berson et al., 1998), 22 epsilon cells (soma size 19.2 μm ±3.1 μm), and 100 delta cells (soma size 19.2 μm ± 2.9 μm).

TABLE 1. Sites of Retrograde Tracer Deposits and Incidence of Ganglion Cell Types in Each Retina

		Cell types					
Retina	Deposit[1]	Eta	Alpha	Beta	Delta	Epsilon	Zeta
CLY13c	SC-contra	1	—	—	5	—	31
CLY13i	SC-ipsi	1	—	—	1	—	—
CLY15c	SC-contra	2	—	—	—	—	11
CLY17c	SC-contra	10	—	—	5	3	5
CLY17i	SC-ipsi	4	—	—	16	—	2
CLY18c	SC-contra	1	—	—	3	—	4
CLY19c	SC-contra	2	—	—	2	—	21
CLY19i	SC-ipsi	3	—	—	5	—	—
CLY20c	SC-contra	11	—	—	1	1	13
CLY20i	SC-ipsi	2	—	—	10	—	—
CLY21i	SC-ipsi	3	—	—	7	—	—
MIN1c	MIN-contra	2	2	35	8	—	—
MIN1i	MIN-ipsi	7	1	12	5	—	—
MIN2c	MIN-contra	1	9	18	2	—	—
MIN4c	MIN-contra	2	3	14	2	19	2
CLAY2L	LGN-C	4	—	—	—	—	—
CLAY3R	LGN-C	9	—	—	—	—	—
CLAY4L	LGN-C	4	2	—	4	11	—
CLAY4R	LGN-C	2	—	—	11	14	—
053096R	—	4	5	—	1	—	22
061896L	—	19	15	1	1	1	20
062496L	—	19	17	3	1	1	24
072596R	—	4	8	—	—	1	3
080796L	—	1	3	26	—	—	5
080796R	—	14	1	6	2	2	11
092096R	—	16	3	3	—	1	11
092096L	—	12	7	—	3	—	11
101696L	—	1	—	2	—	—	—
103096L	—	3	4	—	—	—	—
103096R	—	8	—	—	2	—	5
111396L	—	2	1	3	2	2	—
111396R	—	7	—	4	6	2	4
112696L	—	7	—	4	6	5	19
121196L	—	7	1	1	1	—	8
020697L	—	5	—	1	1	1	6
020697R	—	5	—	—	—	—	2
013197R	—	5	1	—	1	—	1
022697R	—	11	—	1	2	1	17
022697L	—	3	—	1	2	2	10
022297R	—	4	2	—	5	—	4
031997R	—	1	1	4	2	—	1
042397R	—	4	—	5	—	—	4

[1]Sites of retrograde tracer deposit in brain. SC-contra, SC-ipsi: contralateral and ipsilateral superior colliculus; MIN-contra, MIN-ipsi: contralateral and ipsilateral medial interlaminar nucleus of the lateral geniculate nucleus; LGN-C, C laminae of the lateral geniculate nucleus.

Retinas were fixed and processed immunohistochemically as previously described (Pu and Berson, 1992). Some retinas were dehydrated and cleared, and others were coverslipped with 60% buffered glycerol, pH 7.4, without prior dehydration or clearing. Linear shrinkage in the plane of the wholemount was negligible with either method (see Pu et al., 1994). Shrinkage in depth was minimal with the glycerol method; therefore, it was used for all quantitative analyses of stratification. Dry objective lenses were used, so optical foreshortening produced at the air/glass interface (Snell's law) has been corrected by multiplying apparent depth values by 1.52 (Williams and Rakic, 1988). Because of the small difference in refractive index between glycerol (1.47) and glass (1.52), depth values may be overestimated by as much as 5%.

Microscopic analysis

The positions of the area centralis and visual streak were determined from vascular patterns and the densities of ganglion cells, visible from nonspecific histochemical labeling. We estimate that errors in localization were

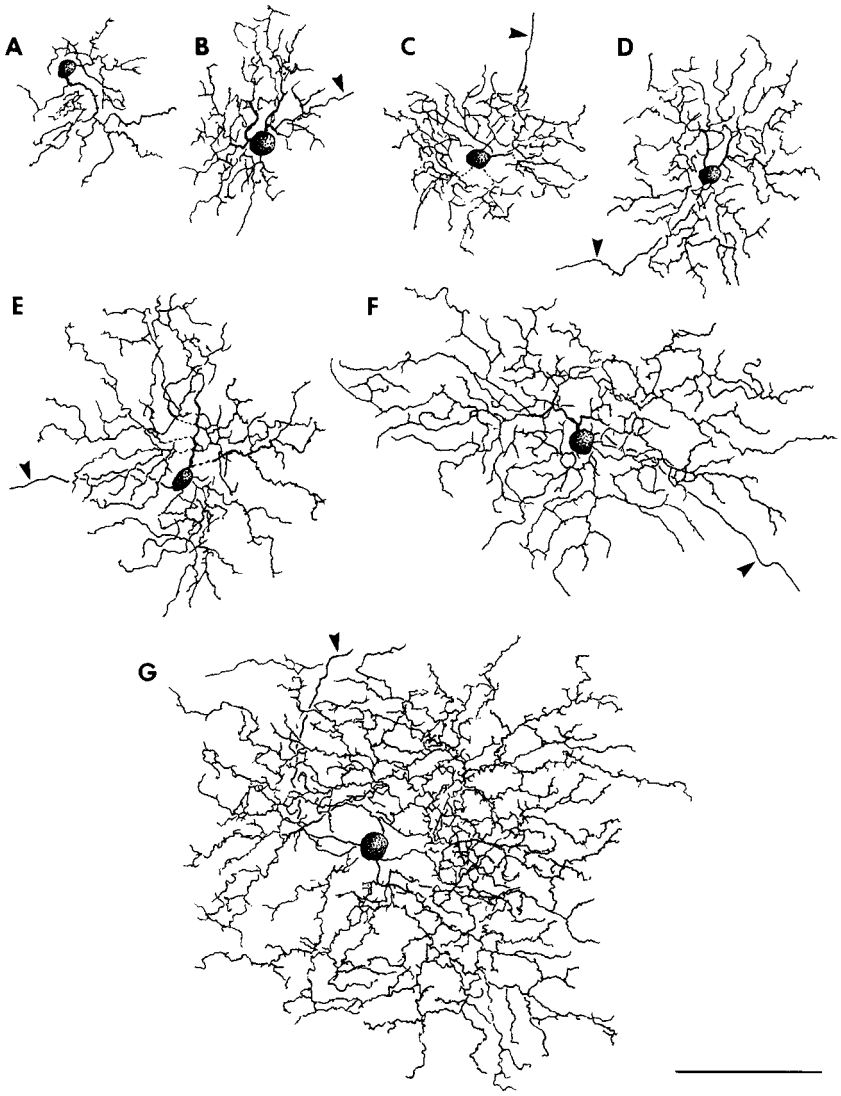

Fig. 1. **A–I:** Camera lucida drawings of stained eta cells in retinal wholemounts. All drawings are at the same scale. Arrowheads indicate axons. Photomicrographs of the cell in G appear in Figure 2A,B, and photomicrographs of the cell in H appear in Figure 2D. Eccentricities (e) and distances from the visual streak axis (s) in millimeters are as follows: A: e = −0.2, s = −0.2; B: e = −0.7, s = 0.0; C: e = −0.8, s = 0.0; D: e = −0.4, s = −0.3; E: e = −1.0, s = −0.4; F: e = +6.0, s = +0.6; G: e = +6.2, s = −5.5; H: e = −9.0, s = +8.4; I: e = +11.5, s = +1.6. Negative eccentricities denote locations in temporal hemiretina, negative streak distances indicate locations in inferior hemiretina. The cell in F was labeled by retrograde transport from the contralateral superior colliculus, and the cell in H was labeled by retrograde transport from the ipsilateral superior colliculus. Scale bar = 100 μm.

<300 μm for the area centralis, <700 μm for the visual streak, and typically much less for both. Axons were distinguished easily from dendrites by their long, unbranched courses, their relatively uniform diameter, and their location in the optic fiber layer, as revealed by through-focus observation. Dendritic field measurements were made only in cells that were judged to be fully stained. To ensure that all dendrites were included regardless of depth, focus was adjusted frequently when plotting the profile. Diameters of dendritic fields and of somata were taken as the mean of the maximal and minimal diameters as measured with an eye-piece graticule. In a small sample of cells, we also estimated dendritic field diameters by a commonly used alternative method. We determined the area of a convex polygon minimally encompassing each cell's dendritic profile (i.e., with its vertices at the tips of the most peripheral processes) and from these calculated equivalent diameters figured as the diameter of a circle equal in area to this polygon. The two methods yielded very similar values: the mean discrepancy was 4.3% ± 4.6% S.D. (n = 12).

A general impression of the depth of dendritic stratification could be obtained by through-focus analysis. Benchmarks for the limits of the inner plexiform layer (IPL) included somata of ganglion and amacrine cells and dark granules marking the distal limit of the IPL (Berson et al., 1998). To our previous discussion of the identity and cellular localization of the granules (Berson et al., 1998), we can add a new observation. The granules are fluorescent in retinas processed for Neurobiotin with fluores-

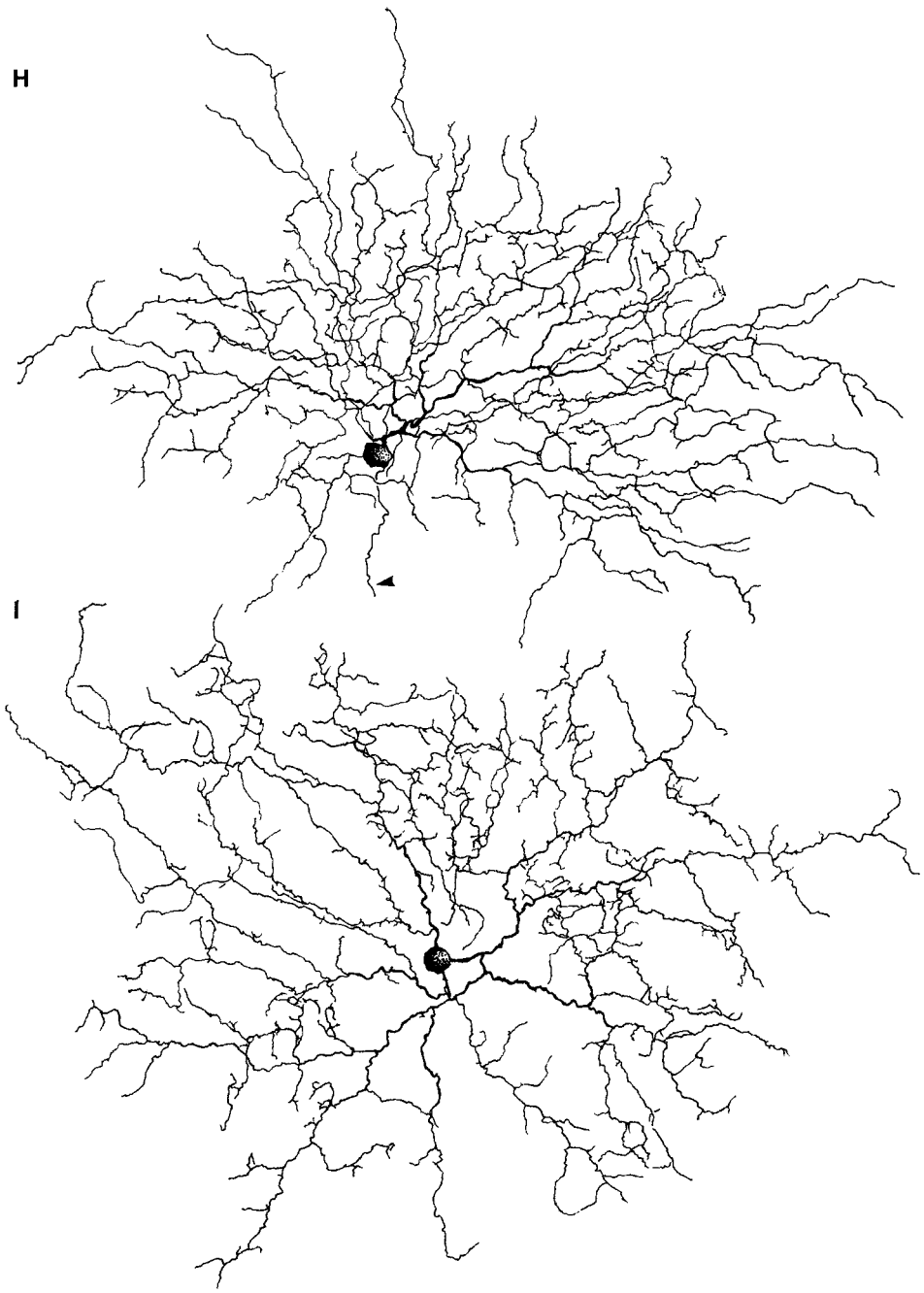

Figure 1 (Continued)

cently tagged streptavidin. Therefore, they seem likely to represent an organelle containing endogenous biotin or a related molecule with avidin binding activity. By using these fiducial marks, it was almost always possible using through-focus analysis to determine with confidence whether a stained alpha or beta cell belonged to the *a* (OFF) or *b* (ON) subtypes. For many of the alpha cells, this judgment could be confirmed because of overlap with another intracellularly stained alpha cell of opposite type. Selected cells were reconstructed in three dimensions by logging the depth of many points along their dendritic profiles. This was done with a digital morphometry system (Neurolucida; MicroBrightfield, Colchester, VT) that included a computer-controlled stage and appropriate software for data acquisition, coordinate transformation, and display.

RESULTS

Eta cells had small somata, slender axons, and highly branched dendritic fields that were intermediate in size among cat ganglion cells (90–590 μm). The camera lucida

drawings of Figure 1 illustrate the form of representative eta cells at various retinal locations. The photomicrographs of Figure 2 display some of the morphologic features of these cells.

Somatic and axonal morphology

Somata were ovoid or round and ranged in diameter from 11–22 μm (mean ± S.D., 15.6 μm ± 2.3 μm; n = 112). Cells within the central 1 mm of the retina tended to have slightly smaller somata, but, otherwise, there was little obvious correlation between soma size and retinal eccentricity (Fig. 3A) or distance from the visual streak (not shown). Eta cells had the smallest cell bodies among known cat ganglion cell types. Their somata were invariably smaller than those of alpha cells stained by the same method and typically smaller than those of beta cells as well (Fig. 2G,I), although there was overlap between the eta and beta distributions (Fig. 3B). Eta cell somata also were significantly smaller on average than those of delta and epsilon cells ($P \ll 0.001$) but were statistically indistinguishable from those of zeta cells ($P > 0.05$; two-tailed t-test, inhomogeneous variances).

Axons of eta cells invariably emerged from the soma. They were typically slender, apparently less than 1 μm in diameter, and comparable in caliber to those of cat zeta cells (Berson et al., 1998). They appeared to be substantially thinner than the axons of beta cells (Fig. 2H,J) and slightly thinner on average than those of epsilon and delta cells stained by the same methods. Some eta cell axons possessed one or two short side branches of the sort seen much more frequently on zeta cell axons (Berson et al., 1998).

Dendritic morphology

Dendritic arbors were compact and densely branched. Typically, one to four primary dendrites emerged from the soma. Most of the dendritic field consisted of very slender processes that were much thinner than the dendrites of alpha, beta, epsilon, and delta cells (Fig. 2B–D). Dendrites of low branch order were often thicker, particularly in peripheral retina, where fields were largest. Dendrites were generally fairly smooth, although some exhibited varicosities or short spines. Branching was abundant and occurred with relatively high frequency in the periphery of the field, a pattern that has been called "tufted" (Ramón-Moliner, 1962; Famiglietti, 1992). Overall, dendrites coursed centrifugally from the soma, but many branches were moderately wavy, and some recurved. Dendritic overlap was a prominent feature of most cells, although its abundance varied from place to place within an arbor and from cell to cell. Arbors were generally compact, and perimeters were well defined, although isolated branches sometimes protruded. Fields were typically circular in form, although some were moderately ellipsoid (Fig. 1F,H). Most somata were centered within the arbor's perimeter, but some were eccentric (Fig. 1A,B,H).

Topographic variations in dendritic field size

Topographic variations in dendritic field size were analyzed in terms of retinal eccentricity (radial distance from the center of the area centralis) and distance superior or inferior from the visual streak, a horizontal band of elevated ganglion cell density that passes through the area centralis (Hughes, 1977). Field size was strongly related to eccentricity (Fig. 4A), ranging from about 100–200 μm in the central retina to about 300–600 μm in the periphery. The proportional increase in field size from the area centralis to the nasal nonstreak periphery (3.5-fold) was comparable to that for alpha, delta, epsilon, and zeta cells but was substantially smaller than that for beta cells (greater than eightfold; Boycott and Wässle, 1974; Kolb et al., 1981; Dacey, 1989; Pu et al., 1994; Berson et al., 1998).

There was also some evidence for a correlation between field size and distance from the visual streak. For example, a plot of eta cell field size against distance from the axis of the visual streak (Fig. 4B) shows that all of the cells with the smallest fields (<200 μm diameter) lay near the streak, whereas all of the cells that lay far from the streak (>5 mm) had large fields (>300 μm diameter). However, distance to the streak accounted for less of the variability in field size ($r^2 = 0.53$) than did eccentricity ($r^2 = 0.64$). Because the visual streak passes through the area centralis, the eccentricity of a cell and its distance from the visual streak are not independent parameters. Cells far from the visual streak, by definition, also are far from the area centralis. Therefore, the strong influence of eccentricity on field size (Fig. 4A) ensures at least a weak correlation between field size and distance from the streak (Fig. 4B). The question thus arises whether cells in nonstreak retina have large fields simply because of their large eccentricities or rather at least partly because of an independent influence of streak distance. One way to disentangle these parameters is to consider the correlation between streak distance and field size for a set of cells all lying at about the same eccentricity. In Figure 4A, consider cells in the nasal hemiretina with eccentricities of 5–10 mm. Those cells lying nearest the visual streak axis (Fig. 4A, solid diamonds) tended to have smaller fields that those lying farthest from it (Fig. 4A, open circles), but there was substantial overlap between these groups. Likewise, in Figure 4B, note that cells at eccentricities greater than 8 mm (Fig. 4B, open circles) had nearly the same field sizes whether they lay near the axis of the streak or in the nonstreak periphery. Taken together, these findings suggest that distance from the visual streak exerts relatively little independent influence on field size. There were no obvious differences in field size between nasal and temporal retina (Fig. 5; see also Fig. 4A,B) nor between superior and inferior hemiretinas (not shown).

Figure 6 compares dendritic field sizes of eta cells with those of the other well-established classes of cat ganglion cells. Eta cell fields (Fig. 6, solid diamonds) were intermediate in size between those of alpha cells (Fig. 6A, open circles) and beta cells (Fig. 6A, solid dots), with very little overlap among the three populations. Field diameters were typically two to three times larger for eta cells than for beta cells and about one-third smaller for eta cells than for alpha cells. Figure 6B compares the field sizes of eta cells with those of the zeta and delta (monoamine-accumulating) ganglion cell types of cat retina. On average, field diameters were typically about 25% smaller for eta cells (Fig. 6B, solid diamonds) than for delta cells (Fig. 6B, open triangles), but there was substantial overlap between the types. There was almost complete overlap between the eta and zeta cell populations (Fig. 6B, open squares), except in the nasal periphery, where the smallest zeta fields, which occupy the visual streak (Berson et al., 1998), are smaller than any of the eta fields.

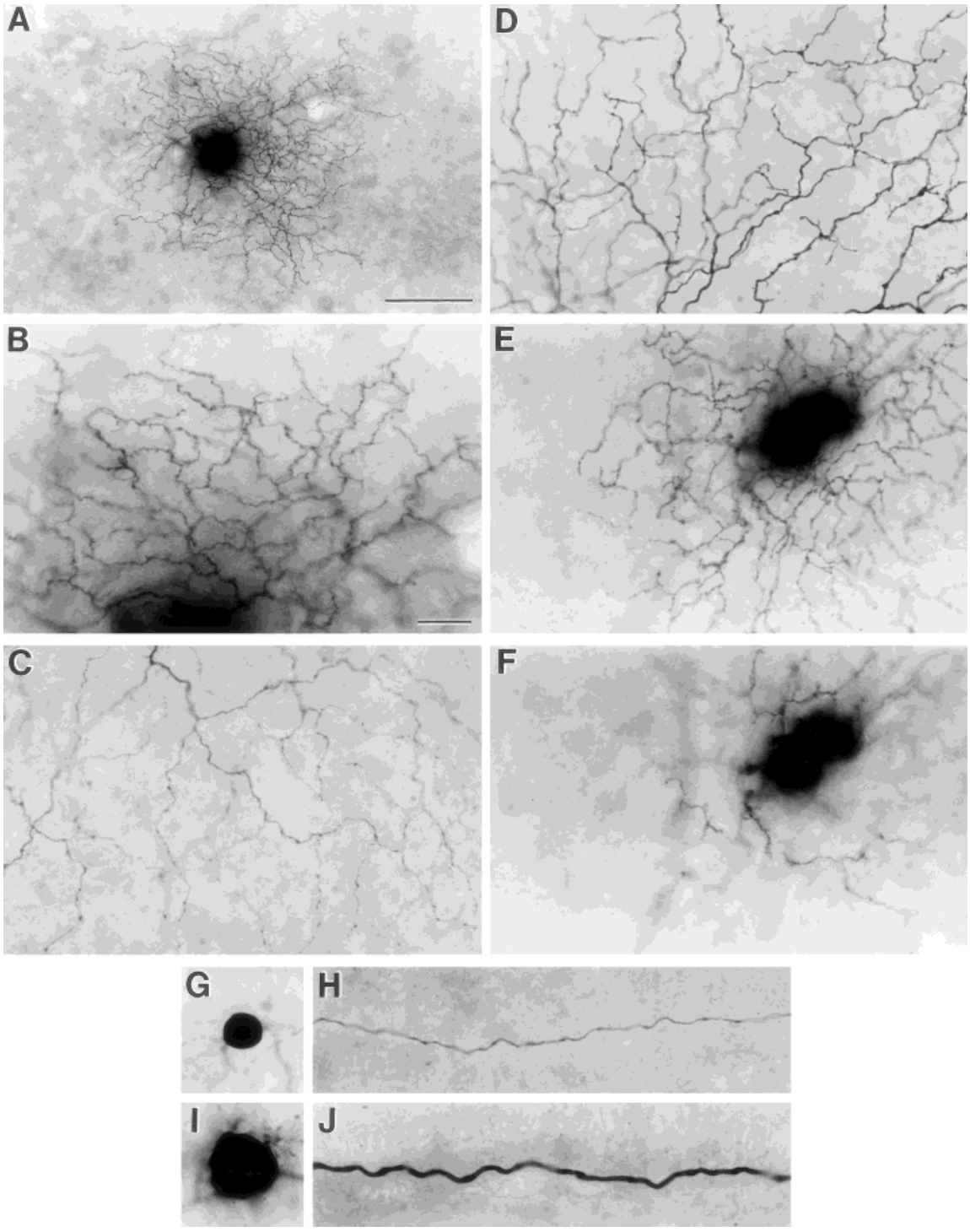

Fig. 2. Photomicrographs illustrating morphologic details of intracellularly stained eta cells. **A,B:** An eta cell as seen at low (A) and high (B) magnification. **C,D:** High-power photomicrographs of dendritic arbors in two other eta cells. **E,F:** Photomicrographs of a single eta cell taken at different focal planes. Plane of focus in E is on the main level of dendritic stratification in S2; plane of focus in F is slightly more proximal at the depth of lower order dendrites in or near S3. **G,H:** Soma (G) and axon (H) of representative eta cells. **I,J:** Soma (I) and axon (J) of representative beta cells for comparison with their topographically matched eta cell counterparts in G and H. Distance from soma to axonal segments illustrated is 350 μm in H and 1.3 mm in J. Eccentricities (e) and distances from the visual streak (s) for illustrated cells as follows, with conventions as described for Figure 1: A,B: e = +6.2, s = −5.5; C,H: e = +8.4, s = +6.5; D: e = −9.0, s = +8.4; E,F: e = −0.9, s = −0.2; G: e = −4.9, s = +0.6; I: e = −3.6, s = +0.7; J: e = +8.8, s = +4.1. The cell in D was labeled by retrograde transport from the ipsilateral superior colliculus. A drawing of the cell in A and B appears in Figure 1G, and a drawing of the cell in D appears in Figure 1H. Scale bars = 100 μm in A, 20 μm in B (also applies to C–J).

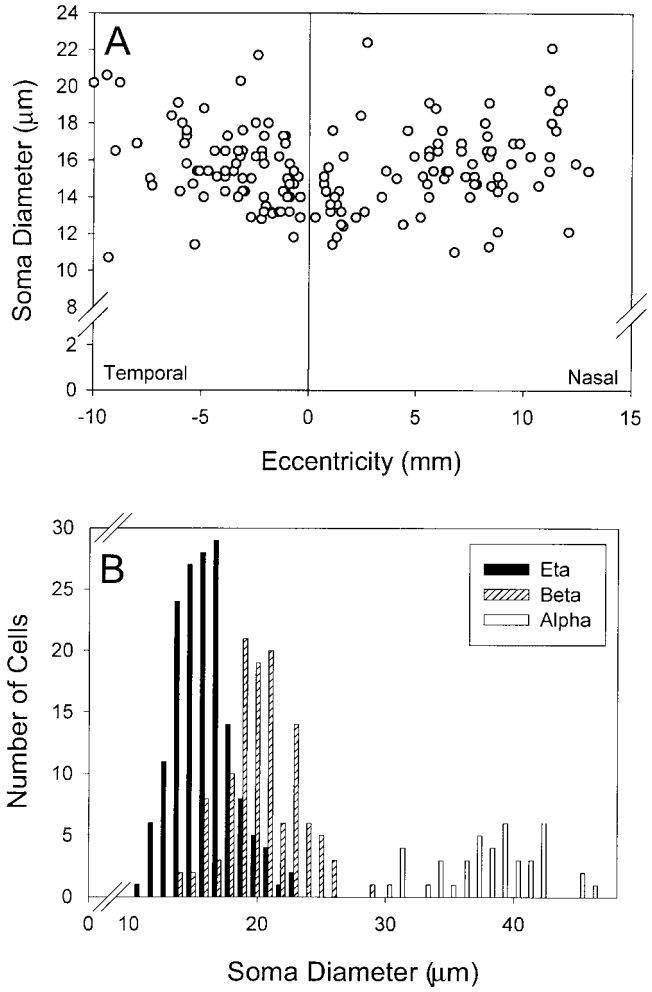

Fig. 3. Soma diameters of eta cells. **A:** Scatter plot of soma diameter as a function of eccentricity. **B:** Histogram comparing soma diameters of eta cells (solid bars) with those of beta cells (hatched bars) and alpha cells (open bars) stained by using identical methods.

Dendritic stratification

Eta cell dendritic arbors ramified broadly within sublamina *a* (the OFF sublayer) of the IPL, whereas none arborized principally in sublamina *b*. Thus, eta cells appear to be an unpaired type rather than comprising a paramorphic pair of types (i.e., types virtually identical when viewed en face but differing in the level of their dendritic stratification in the IPL; Famiglietti and Kolb, 1976).

The stratification in sublamina *a* was relatively broad. This was evident in hydrated wholemounts from the difference in focal depth of several micrometers between overlapping distal branches. The most sclerad branches appeared to occupy S1, abutting the inner nuclear layer, but most processes appeared to lie in S2. Dendrites of low branch order often coursed in sublamina *b* for substantial distances before joining the main arbor in sublamina *a* (Fig. 2E,F). Figure 7 documents these features for one eta cell that was reconstructed by computer and is displayed as if viewed along an axis in the plane of the retina. This cell was unusual in possessing two short dendritic branches that apparently terminated in sublamina *b*.

To determine more accurately the level of stratification, we used through-focus methods to compare the depths of eta cell dendrites with those of overlapping fiducial ON- and OFF-alpha cells (Figs. 8–10). Eta cell dendrites exhibited extensive costratification with the arbors of type *a* (OFF) alpha cells in S2 (Figs. 8, 9E–I, 10D–G). In most cases, they also ramified partly sclerad to the OFF-alpha arbor, that is, in S1 (Figs. 8C, 9G,I, 10D,F). More rarely, eta cell processes were found just proximal to those of OFF-alpha cells (Fig. 10D,F) near the *a*/*b* sublaminar border. Except for primary dendrites en route to sublamina *a*, it was very rare to find eta cell processes arborizing at or proximal to the depth of ON-alpha cell dendrites (S3/S4), although we did encounter a few examples (see, e.g., Figs. 7, 9D,F,H). These observations were based on 16 eta cells, of which five overlapped both ON- and OFF-alpha cells and 11 overlapped one of the two types.

We confirmed the foregoing analysis by using other ganglion cell types as fiducial cells. Delta (monoamine-accumulating) cells are known to ramify exclusively in S1 (Dacey, 1989; our own unpublished observations; however, see also Wässle and Boycott, 1991). In each of eight cases, eta cells costratified at least partly with an overlapping delta cell; typically, the eta cell also arborized just proximal to the delta cell in S2 (Fig. 10). The dendrites of zeta cells stratify narrowly near the *a*/*b* sublaminar border (Berson et al., 1998). In six instances of overlap, eta cell dendrites invariably ramified distal to the zeta cell dendrites, although, in two examples, it appeared that there was also modest costratification. OFF-beta cells stratify broadly in sublamina *a*, and ON-beta cells stratify mainly in S3 and S4 (Famiglietti and Kolb, 1976; Watanabe et al., 1985; McGuire et al., 1986; Weber et al., 1991). Eta cell dendrites largely costratified with those of OFF-beta cells (n = 3) and ramified almost entirely sclerad to those of ON-beta cells (n = 3). Eta cell dendritic arbors lay entirely distal to overlapping epsilon arbors (n = 4), which are known to occupy S3 and S4 (Pu et al., 1994). Together, these data indicate that eta cell terminal dendrites arborize broadly in sublamina *a*, from the inner nuclear layer to the *a*/*b* sublaminar border, with perhaps a few wayward branches in sublamina *b*.

Mosaic and density distribution

Lacking a method for marking eta cells selectively, we were unable to reveal their mosaic by staining all cells of this type in a patch of retina. However, by chance, we did stain three pairs of eta cells with overlapping dendritic fields. Such overlap suggests that eta cell dendritic field overlap or coverage factor (dendritic field area × local density) is at least one. The best stained cell pair is illustrated in Figure 11. The interdigitation of the dendrites of the two cells suggests that eta cells may completely tile the retina with minimal overlap. More extensive eta cell overlap cannot be excluded, however, because we cannot be certain that we injected nearest neighbors in the eta-cell mosaic.

By assuming that dendritic field area is inversely proportional everywhere to the local density of eta cells, as is true for other ganglion cell types (Peichl and Wässle, 1979; Wässle et al., 1981; Dann et al., 1988; Dacey, 1989, 1993b; Vaney, 1994; Stein et al., 1996), we used field sizes to derive estimates of local eta cell density. For each of 219 cells, we generated a local estimate of eta cell density by

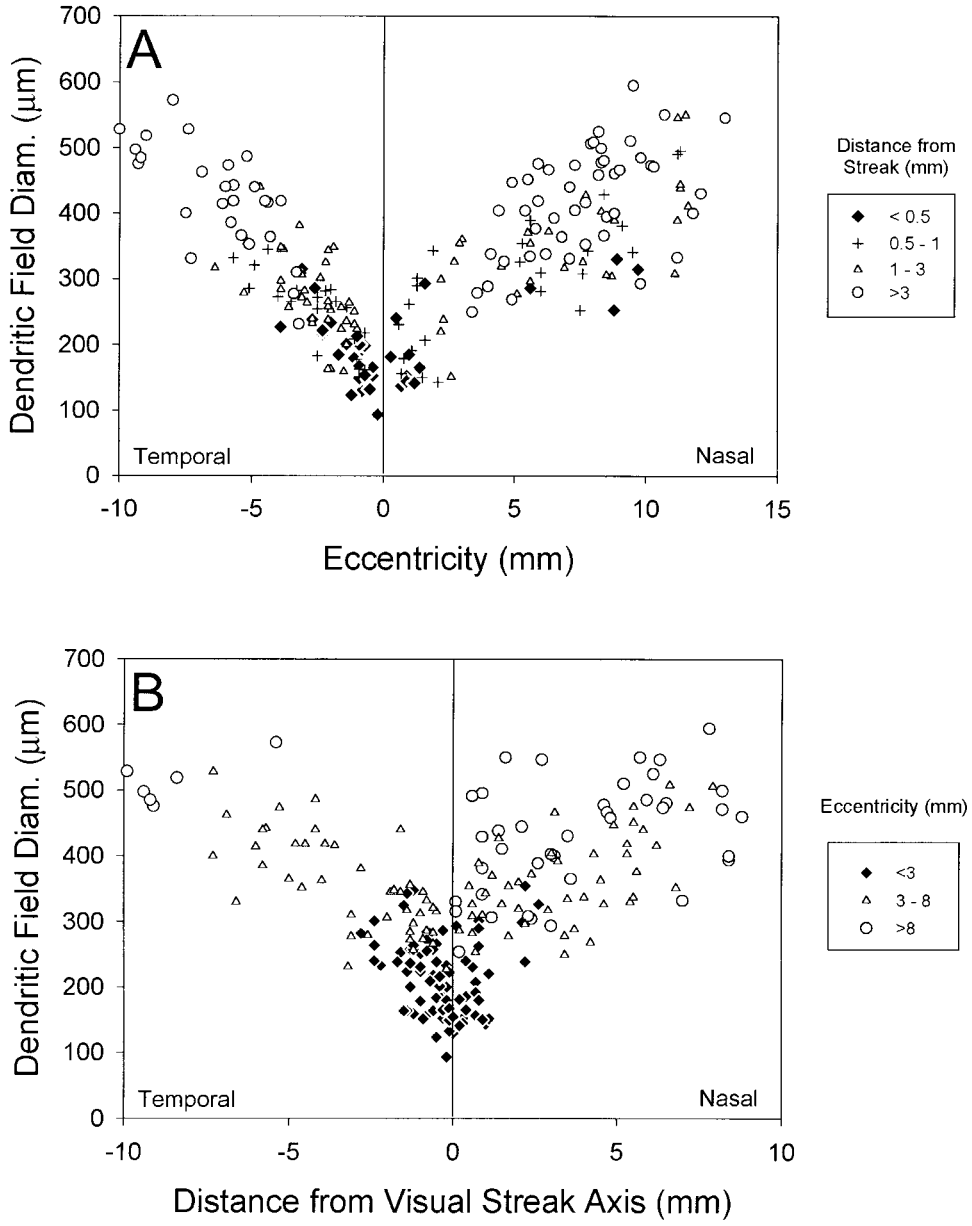

Fig. 4. Dependence of eta cell dendritic field size on retinal eccentricity and distance from the visual streak. **A:** Plot of field diameter as a function of eccentricity (i.e., radial distance from the area centralis). Each symbol type indicates a range of distance from the axis of the visual streak, as indicated in the key. **B:** Plot of field diameter as a function of distance from the visual streak axis. Each symbol type indicates a range of eccentricity, as indicated in the key. In both A and B, a negative sign has been assigned to distance values (abscissa) for cells in the temporal hemiretina. No distinction has been made between superior and inferior retinal locations.

dividing 1 (a rough estimate of the coverage factor) by the dendritic field area of the cell. These density estimates, which are summarized in the contour plot of Figure 12 (left), ranged from 146 cells/mm^2 in the central retina to 4 cells/mm^2 in the nasal periphery. Although the magnitudes of the estimated densities are subject to the imprecision of the estimate of coverage factor, the form of the distribution presumably closely matches that of the true distribution provided that the assumption of topographic invariance of coverage is correct. The isodensity contours are moderately ellipsoid with their long axis nearly horizontal, suggesting that these cells show some tendency to concentrate in the visual streak. However, this tendency is far weaker than for certain other cat ganglion cell types, particularly the zeta cell (Fig. 12, right).

Central projections

Eta cells were encountered commonly among cells labeled by retrograde transport from the superior colliculus (n = 41; for examples, see Fig. 1F,H) and from the medial interlaminar nucleus (n = 12) and C laminae (n = 15) of the lateral geniculate nucleus. We observed no clear examples of eta cells among >300 cells labeled from the A

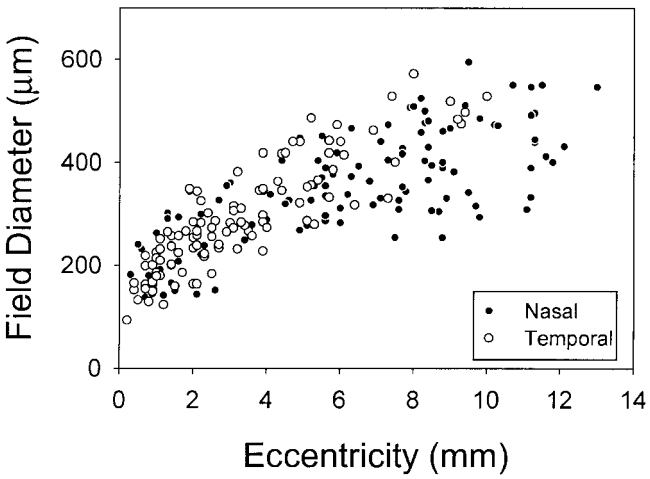

Fig. 5. Comparison between the dendritic field sizes of eta cells in the nasal hemiretina (solid dots) and temporal hemiretina (open circles). The apparent mismatch in the far periphery arises because the temporal hemiretina has a shorter horizontal extent than the nasal hemiretina. The few temporal cells with eccentricities >8 mm lay in the superior or inferior periphery.

layers of the lateral geniculate nucleus nor among >150 cells labeled from the geniculate wing. Eta cells appeared to have uncrossed projections from the temporal retina. Sixteen eta cells were among the several hundred temporal retinal cells labeled from the ipsilateral superior colliculus or geniculate complex, whereas none was among a much smaller sample of cells labeled from the contralateral colliculus.

DISCUSSION

The present study defines a new morphologic type of cat ganglion cell, the eta cell. Its salient morphologic features include a small soma, slender axon, highly branched and compact dendritic field, and broad stratification in sublamina *a* of the IPL. It innervates both the midbrain tectum and the visual thalamus and projects ipsilaterally from the temporal retina.

Comparison with other cat ganglion cell types

The eta cell is clearly distinct from the seven other well-studied morphologic ganglion cell types of the cat retina: the ON- and OFF-alpha cells; the ON- and OFF-beta cells; and the delta (monoamine-accumulating), epsilon, and zeta cells. Each of these meets the definition of a "natural type" (Rodieck and Brening, 1983), in that its members form a relatively distinct cluster of points in multidimensional parameter space. The parameters we have used either implicitly or explicitly to demonstrate the uniqueness of the eta cell include soma size, axon caliber, field size, topographic location, frequency of dendritic branching and overlap, dendritic stratification, and patterns of central projection. The clustering of eta cells and their distinction from members of other types are apparent to varying degrees in the projection of the full parametric space onto one- or two-dimensional plots, such as those in Figures 3B, 6A,B (see also Figs. 9H,I, 10F,G, 13). However, these lower dimensional plots leave substantial overlap among various types. The full parametric space cannot be represented in a way that would permit straightforward recognition of clusters. It is therefore important to specify subsets of parameters ("identification sets" of Rodieck and Brening, 1983) sufficient to distinguish eta cells from other known types.

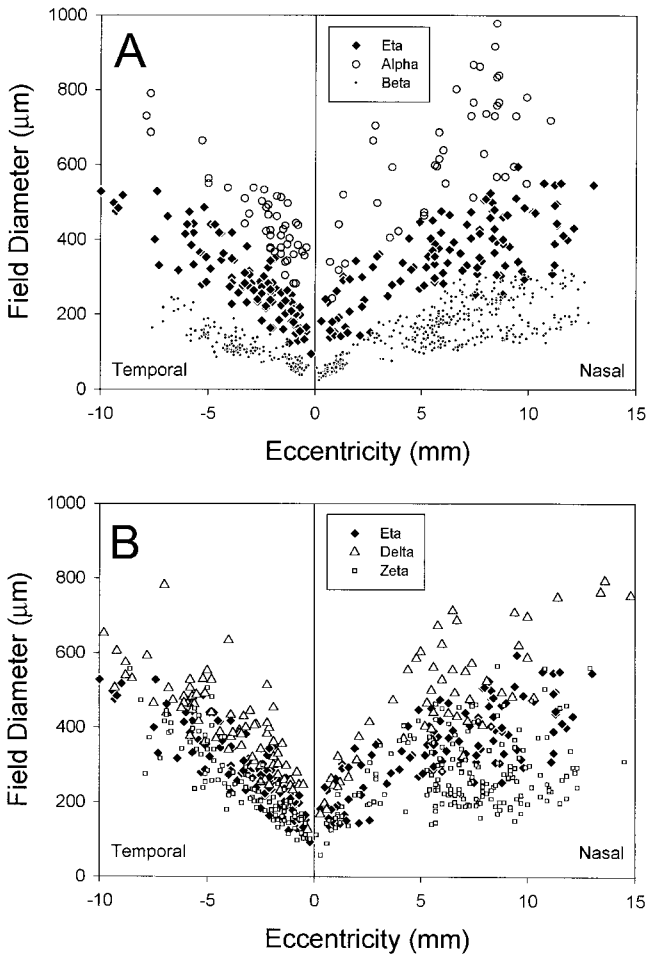

Fig. 6. Comparison of dendritic field sizes of eta cells with those of other types of cat ganglion cells. **A:** Comparison of eta cells (solid diamonds) with alpha cells (open circles) and beta cells (solid dots). **B:** Comparison of eta cells (solid diamonds) with delta (monoamine-accumulating) cells (open triangles) and zeta cells (open squares). For other conventions, see Figure 4.

Alpha cells are readily distinguishable from eta cells on the basis of soma size (Fig. 3B) or axonal caliber alone and from the correlation between dendritic field size and eccentricity (Fig. 6A). For ON-alpha cells, dendritic stratification also is an unambiguous discriminator (Fig. 13). Discrimination of beta and eta cells is easiest by using stratification (ON-beta cells only; Fig. 13) or dendritic field size. The latter cue is sufficient if topographic location is known (Fig. 6A). Otherwise, a relatively large dendritic field (>300 μm diameter), a small soma, or a thin axon will help to identify a cell as belonging to the eta type rather than the beta type. Epsilon and eta cells exhibit entirely distinct patterns of stratification (Fig. 13) and virtually nonoverlapping distributions of dendritic field size at any eccentricity (cf. Fig. 6; Pu et al., 1994). A metric of

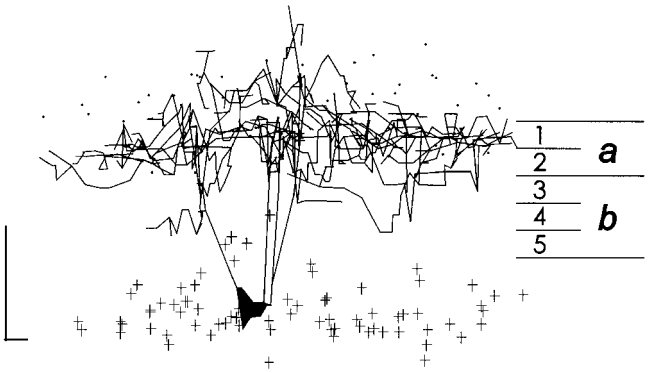

Fig. 7. Dendritic stratification of an eta cell of the central retina as revealed by a computer-generated, transverse view. Dendritic branching was traced in three dimensions in a hydrated wholemount by using a computer-based microscopic reconstruction system then displayed as if it had been rotated by 90° about an axis lying in the plane of the retina. This cell was selected for reconstruction because the relatively small size of its dendritic field reduced the distorting effect of imperfect wholemount flatness on the uniformity of depth information in such views. Cell body appears as a solid polygon, dendrites appear as straight line segments. Plus signs indicate the depth of other ganglion cell bodies, and dots indicate the position of dark granules marking the outer margin of the inner plexiform layer (see Material and Methods). Numbers at the right indicate approximate depth of strata of the inner plexiform layer, and *a* and *b* denote the OFF and ON sublayers, respectively. The cell was located 1.0 mm from the area centralis and 0.4 mm from the visual streak in the inferior nasal retina. Note that the thickness of the retina has been greatly exaggerated in this display. Scale bar = 10 μm (applies to both vertical and horizontal dimensions).

branching density would presumably be nearly as good a discriminator.

Delta and zeta cells are perhaps the hardest types to distinguish from eta cells given the substantial overlap among these types along several of the dimensions considered in this report. For these types, close inspection of dendritic stratification patterns will be of greatest diagnostic value. Whereas eta cell arbors ramify heavily in S2 (along with OFF-alpha arbors), delta arbors lie almost entirely distal to this sublayer, and zeta arbors lie just proximal to it (Dacey, 1989; Berson et al., 1998; Figs. 10, 13). In cases in which analysis of stratification is precluded, discrimination of these types generally requires assessment of multiple features. On average, compared with eta cells, delta cells have larger dendritic fields, larger somata, and thicker axons and dendrites. Their dendritic trees are more planar, more radiate and regular, and more sparsely branched than those of eta cells, with less dendritic overlap (Wässle et al., 1987; Dacey, 1989; Fig. 10C). Zeta cells typically have smaller dendritic trees than eta cells, particularly within the visual streak (Fig. 6B; Berson et al., 1998). They also have more planar, less highly overlapped dendritic fields and are more likely to exhibit spines and other dendritic specializations. They apparently lack the uncrossed ipsilateral projection and thalamic terminations of the eta cells (Berson et al., 1998).

Other than the alpha, beta, epsilon, and delta cell types, a great variety of less thoroughly studied morphologic forms has been depicted in earlier reports on cat ganglion cells (see, e.g., Boycott and Wässle, 1974; Stone and Clarke, 1980; Kolb et al., 1981; Saito, 1983; Fukuda et al., 1984; Stanford, 1987; Ramoa et al., 1988; Tootle, 1993). Among these, two may correspond to the eta type described here. One, a physiologically characterized cell in the study of Stanford (1987), is discussed in detail below. The other is the cell termed G6 in the Golgi survey of Kolb et al. (1981). That cell resembled the eta cell, in that it had a small soma; slender, densely branched dendrites; a field of about the right size (≈130 μm diameter at 0.5 mm eccentricity); and dendritic ramification in sublamina *a*. However, the G6 cell apparently was stratified more narrowly than the eta cell, being confined to stratum 2.

Likely homologues of the eta cell in other mammalian retinas

A ganglion cell resembling the eta cell is present in the retina of the ferret, a carnivore that shares many features of retinal organization with the cat. Like the cat eta cell, this ferret ganglion cell type has a small soma, fine axon, and highly branched, overlapping dendritic field of intermediate diameter ramifying broadly in sublamina *a* (Isayama et al., 1998). Ferret eta cells are likely to have been encountered originally by Wingate et al. (1992), who apparently included them in the heterogeneous group of ganglion cells they designated "tight" (see especially cells ii and v in their Fig. 9). However, the tight group probably consists of multiple cell types, including a counterpart of the cat zeta cell (Berson et al., 1998; Isayama et al., 1998). The population of ganglion cells projecting to the ipsilateral midbrain and thalamus includes eta cells in the cat but apparently does not include "tight" cells (presumably including eta cells) in the ferret (Wingate et al., 1992). It is unclear whether this reflects a real species difference, because the data set in the ferret study was relatively small.

It is less certain that the eta cell type has counterparts in the retinas of other mammalian orders. Possible homologues of the eta cell can be seen among the "T group" of tectally projecting ganglion cells stained by Rodieck and Watanabe (1993; cell at lower left and possibly upper right of their Fig. 8). However, unlike the cat eta cell, these cells were reported to be fully bistratified, with complete arbors in both the *a* and *b* sublaminae. Surveys of ganglion cell morphology in the rabbit retina (Famiglietti, 1992; Amthor et al., 1989a,b) include no obvious equivalents of the eta cell.

Distribution of eta cells

At present, we lack a method for selectively labeling eta cells that would permit direct assessment of their retinal distribution. Nonetheless, inferences about the form of their density distribution can be drawn from the topography of their dendritic field sizes by assuming that their dendritic field overlap or coverage factor (field area × local density) is a constant (Peichl and Wässle, 1979; Wässle et al., 1981; Dann et al., 1988; Dacey, 1989, 1993b; Vaney, 1994; Stein et al., 1996). We assumed a coverage constant of 1, because the data of Figure 11 suggest that eta cells completely tile the retina with minimal overlap. This may underestimate eta cell coverage, because we may never have successfully injected nearest neighbors in the eta cell mosaic. Coverage appears to be greater than 1 for most cat ganglion cell types studied to date (Peichl and Wässle, 1979; Wässle et al., 1981; Dacey, 1989; Stein et al., 1996; Berson et al., 1998). Note, however, that, although under-

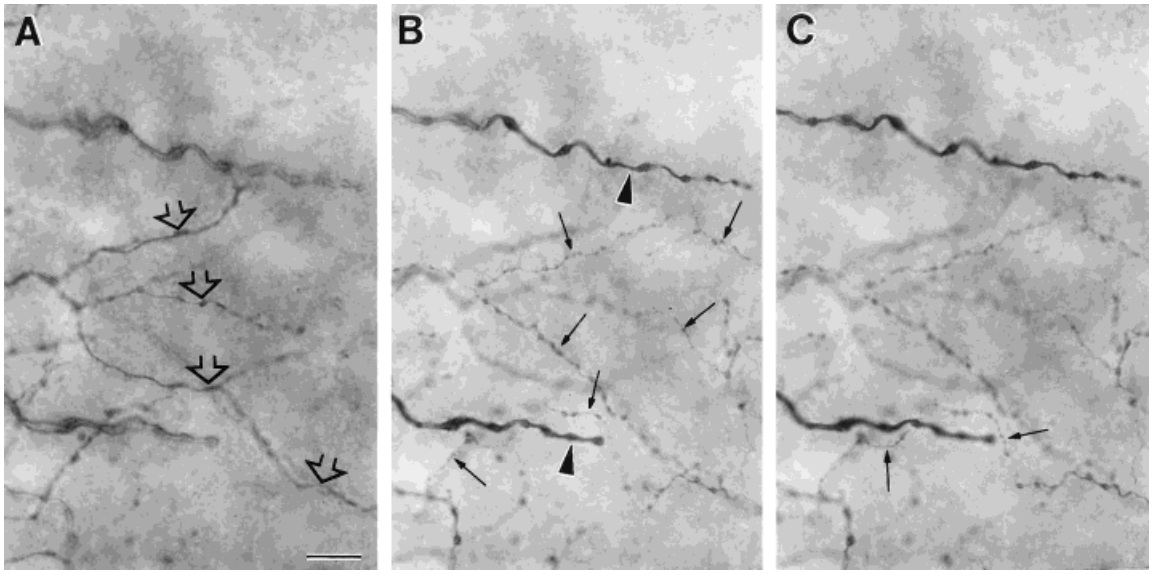

Fig. 8. **A–C:** Through-focus series of photomicrographs comparing depth of dendritic stratification of an eta cell, an ON-alpha cell, and an OFF-alpha cell with mutually overlapping arbors. Plane of focus is most proximal in A, most distal in C. The focal plane in A corresponds to the level of stratification of the ON alpha cell dendrites (open arrows). Focal plane in B lies approximately 4 μm distal to that in A and corresponds to the level of stratification of the OFF-alpha dendrites (arrowheads) and also of most of the dendrites of the eta cell (arrows). Arrows in C mark slender eta cell dendrites apparently ramifying just distal to a thicker OFF-alpha dendrite. For additional data on this set of overlapping cells, see Figure 10. Scale bar = 10 μm.

estimating coverage would lead to proportional underestimation of density, it would not distort the form of the distribution shown in Figure 12.

There are three noteworthy features of this distribution. First, the isodensity contours exhibit only a modest horizontal elongation, indicating a relatively weak tendency of these cells to concentrate in the visual streak. For example, outside the central retina, the ratio of width to height for these contours is <2 for eta cells, whereas it ranges from 2.1 to 2.8 for ganglion cells considered collectively (Wong and Hughes, 1987), and it approaches or exceeds 4 for zeta cells, a cell type that is highly concentrated in the streak. Second, the eta cell distribution is more symmetric about the nasotemporal raphe than is true for other ganglion cell classes. For example, at 5 mm horizontal eccentricity, the ratio of nasal to temporal densities is about 1.3 for eta cells (Fig. 12) compared with about 1.7 for delta cells (Dacey, 1989), 2 for beta cells (Stein et al., 1996), and about 2.5 for zeta cells or for all ganglion cells combined (Wong and Hughes, 1987; Berson et al., 1998). Finally, the gradients in cell density are shallower for eta cells than for ganglion cells overall. For example, at 10 mm eccentricity in the nonstreak nasal retina, estimated eta cell density is fully 8% of that in the area centralis, whereas overall ganglion cell density is only 2% of its peak value in the central retina (Wong and Hughes, 1987). This discrepancy may be traced in part to the fact that beta cells, which constitute more than half of the ganglion cell population, are represented disproportionately in the central retina (Stein et al., 1996).

Fig. 9. Comparisons of depth of dendritic stratification of three cells with overlapping dendritic arbors: an eta cell, an ON-alpha cell, and an OFF-alpha cell. A–C: Camera lucida drawings of the three cells. **A:** ON-alpha cell. **B:** OFF-alpha cell. **C:** Eta cell. Somatic outlines of the ON-alpha cell and the eta cell have been included in B to show the actual spatial relationships of the three cells. The drawings in A and C have been shifted horizontally (arrows) in relation to that in B to show the morphology of the three cells in isolation. Axons were omitted for clarity. The eta cell was located 5.4 mm from the area centralis and 5.3 mm from the visual streak axis in the inferior nasal retina. D–I: Quantitative analysis of relative depth of stratification of these cells. **D:** Computer-generated, transverse view of the fully reconstructed arbor of the eta cell shown in C (for conventions, see Fig. 7, except that the soma is represented as an ellipse). **E:** Absolute depth of dendrites of the eta cell (open diamonds), the ON-alpha cell (open circles), and the OFF-alpha cell (solid circles). Data are plotted as a function of linear distance on the retina to produce a radial view comparable to that in D. Each point represents the depth of a dendrite at an intersection between the dendritic profiles of two of these cells. The dendrites of the eta cell can be seen to ramify generally at about the same depth as those of the OFF-alpha cell, but undulations in the wholemounted retina introduce noise in the depth data that partly obscure the relationship. **F:** Subset of the data in E replotted by normalizing values to the depth of overlapping ON-alpha dendrites to flatten the tissue warp evident in D and E. The eta cell largely costratifies with the OFF-alpha cell in or near S2; however, at several points (nearly all associated with a single dendritic branch), it stratifies with or just proximal to the ON-alpha cell. **G:** Subset of the data in E replotted by normalizing values to the depth of overlapping OFF-alpha dendrites. Eta cell dendrites appear to costratify with OFF-alpha dendrites or to lie just distal to them. Because all depth measurements were made at points of intersection of two dendritic profiles (and never of all three), the data in F and G represent mutually exclusive subsets of the data in E. For example, points in F showing modest costratification of the eta cell and the ON-alpha cell are absent from G because nearly all were derived from a single dendrite that did not intersect the OFF-alpha profile. **H,I:** Histograms displaying the normalized depth data from F and G, respectively. Scale bars = 100 μm in A–C, 10 μm vertically and 50 μm horizontally in D (also applies to E–G).

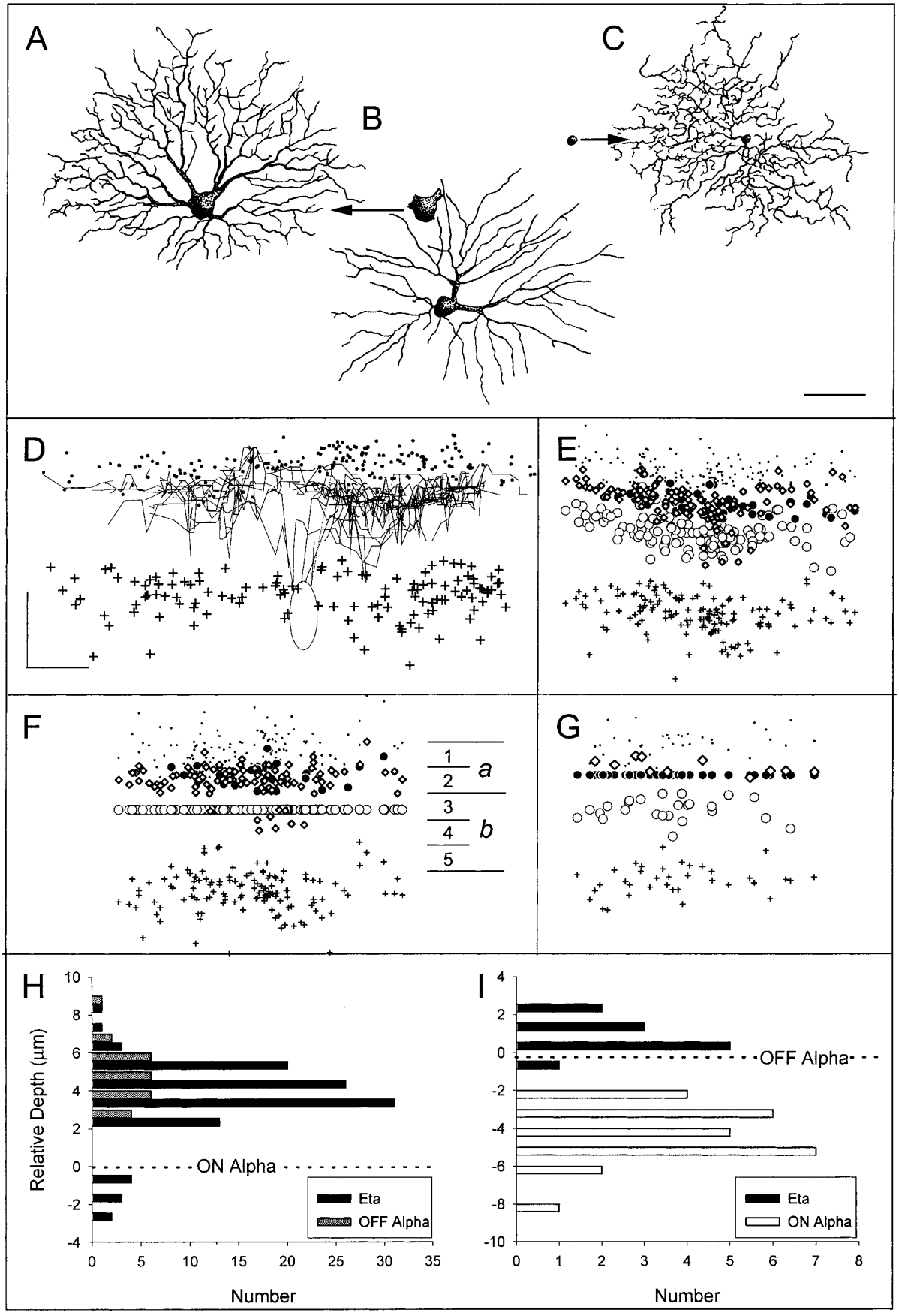
A
B
C
D
E
F
G
1
2
a
3
4
b
5
H
Relative Depth (μm)
ON Alpha
Eta
OFF Alpha
Number
I
OFF Alpha
Eta
ON Alpha
Number

Figure 9

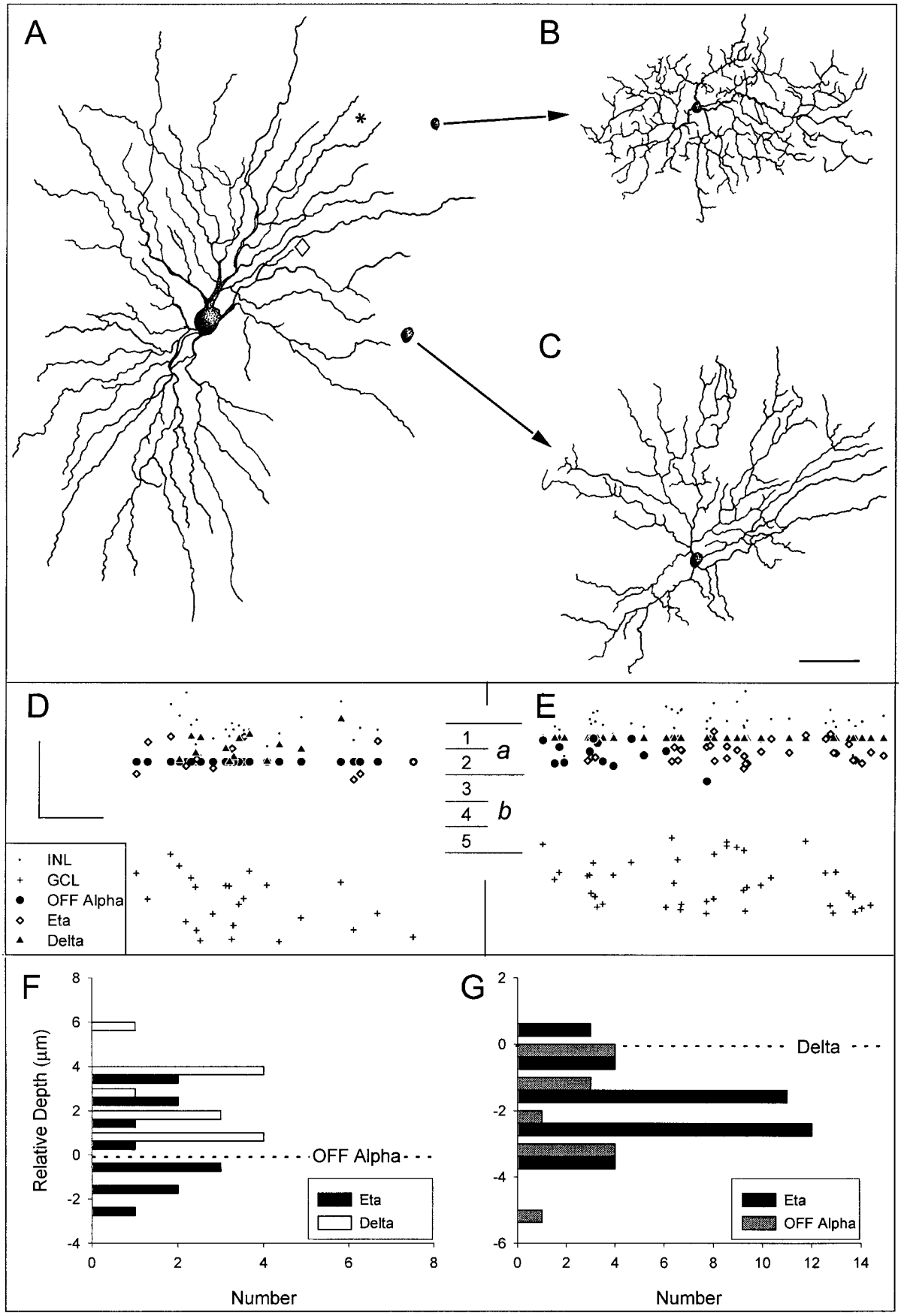
A
B
C
D
E
1
2
a
3
4
b
5
INL
GCL
OFF Alpha
Eta
Delta
F
Relative Depth (µm)
OFF Alpha
Eta
Delta
Number
G
Delta
Eta
OFF Alpha
Number

Figure 10

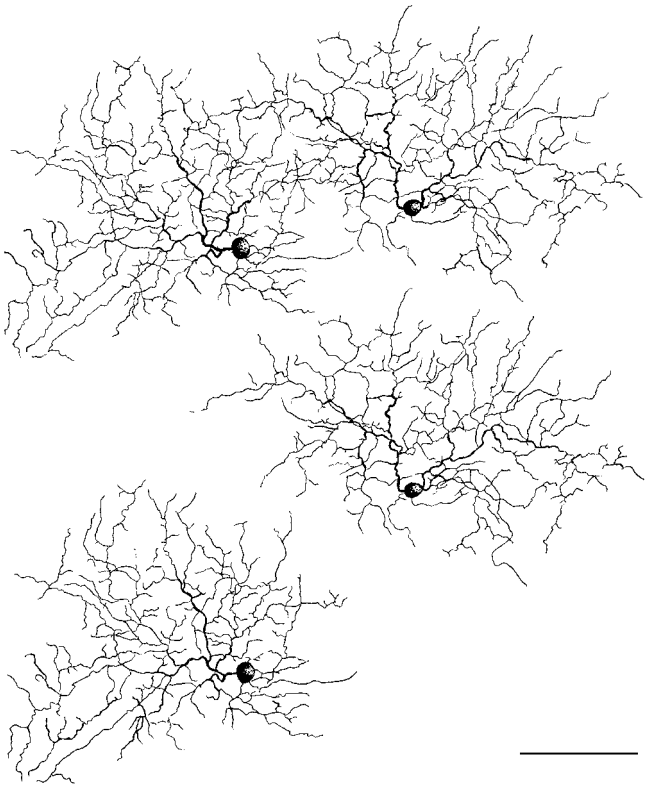

Fig. 11. Camera lucida drawings of an example of dendritic overlap between two neighboring eta cells. The cells are shown in their actual spatial relationship above and separately below. The cells were located 5.0 mm from the area centralis and 0.7 mm from the axis of the visual streak in the superior temporal retina. Axons were omitted for clarity. Scale bar = 100 μm.

Relative incidence and total numbers of eta cells

The incidence and total numbers of eta cells can be estimated only indirectly at this point, pending the development of a selective staining method. Integration of the inferred eta cell density distribution (Fig. 12A) yields an estimated total of 5,000 eta cells per retina. This amounts to 3% of the estimated total ganglion cell population of about 160,000 (Williams et al., 1983; Chalupa et al., 1984). This should be viewed as a lower-bound estimate of the numbers of eta cells, because it is based on a conservative estimate of eta cell coverage.

Physiologic identity

The ample numbers of eta cells makes it likely that they have been encountered in physiologic studies (Cleland and Levick, 1974a,b; Stone and Fukuda, 1974; Rowe and Stone, 1976; Troy et al., 1989; Rowe and Palmer, 1995). Because they are distinct from both alpha and beta cells morphologically, they are presumably neither Y nor X cells physiologically and correspond instead to one of the W cell or sluggish types. The slender axon of the eta cell is consistent with this view, because it implies a slow axonal conduction velocity, a property typical of W cells or sluggish cells (Stone, 1983).

Given their stratification almost exclusively within sublamina *a*, eta cells seem likely to have OFF-center receptive fields (Famiglietti and Kolb, 1976; Wässle and Boycott, 1991; Rodieck, 1998). There are two main varieties of OFF-center W cells that can be distinguished by the temporal profile of their response to changes in luminance within the receptive field center. One variety, termed the OFF-center phasic W (Stone and Fukuda, 1974) or OFF-center sluggish transient (Cleland and Levick, 1974a), responds to prolonged luminance decrements with only a brief initial burst of spikes. The other variety, termed OFF-center tonic W (Stone and Fukuda, 1974) or OFF-center sluggish sustained (Cleland and Levick, 1974a), increases its discharge rate for the duration of the dark stimulus.

There is some anatomic evidence to suggest that, of these two, the phasic variety is the more likely counterpart of the eta cell. Eta cells have among the slenderest axons and smallest somata of any cat ganglion cells we have stained, properties more in keeping with those of phasic W cells than of tonic W cells (Cleland and Levick, 1974a,b; Stone and Fukuda, 1974; Rowe and Stone, 1976; Stanford, 1987). By comparison, the monoamine-accumulating delta cell has a relatively large soma and thick axon (for a nonalpha, nonbeta cell), and seems a better match for the tonic OFF-center W cell.

Preliminary data from whole cell recordings of identified eta cells support the proposed correspondence between eta cells and OFF-center phasic W cells (O'Brien et al., 1999). Further corroboration of the proposed equivalence comes from the structure-function study of Stanford (1987). Of two physiologically identified OFF-phasic W cells that he stained, at least one (illustrated in his Fig. 5E) seems likely to have been an eta cell. Its dendritic arbor, like that of the eta cell, was compact, circular, and densely branching with extensive overlap. The soma was very small, and the axon was slender. The dendritic field was about 260 μm in diameter, within the range of eta cells at this eccentricity (8.4° or about 1.8 mm).

At least two objections may be raised to the proposed correspondence. The first stems from a consideration of patterns of decussation at the optic chiasm. Most phasic OFF-center W cells project contralaterally from the temporal retina (Fukuda and Stone, 1974; Kirk et al., 1976), whereas at least some eta cells (and most tonic OFF-center

Fig. 10. Comparison of depth of dendritic stratification of an eta cell, an OFF-alpha cell, and a delta (monoamine-accumulating) cell. A–C: Camera lucida drawings of the three cells. **A**: OFF-alpha cell. **B**: Eta cell. **C**: Delta cell. The somatic outlines of the eta and delta cells are included in A to show the actual spatial relationships of the three cells. The drawings of their dendritic profiles (B and C) have been shifted (arrows) to show the morphology of the three cells in isolation. Axons were omitted for clarity. The diamond in A indicates the position of the soma of another filled cell in this region, an ON-alpha cell. The ON-alpha cell dendrites are omitted from this analysis but are shown in the photomicrographs of Figure 8, which were drawn from the location indicated by the asterisk in A. The eta cell was located 7.3 mm from the area centralis and 3.0 mm from the visual streak axis in the inferior nasal retina. D–G: Quantitative analysis of the relative depth of dendritic stratification of these three cells. **D,E**: Scatter plots of dendritic depth at points of overlap between dendritic profiles, as for Figure 9F,G. Data are normalized to depth of either the OFF-alpha cell dendrites (D) or the delta cell dendrites (E). **F,G**: Normalized depth data of D and E replotted as histograms. Eta cell processes appear to costratify with the dendrites of both the OFF-alpha cell and the delta cell. INL, inner nuclear layer; GCL, ganglion cell layer. Scale bars = 100 μm in A–C, 10 μm vertically and 50 μm horizontally in D (also applies to E).

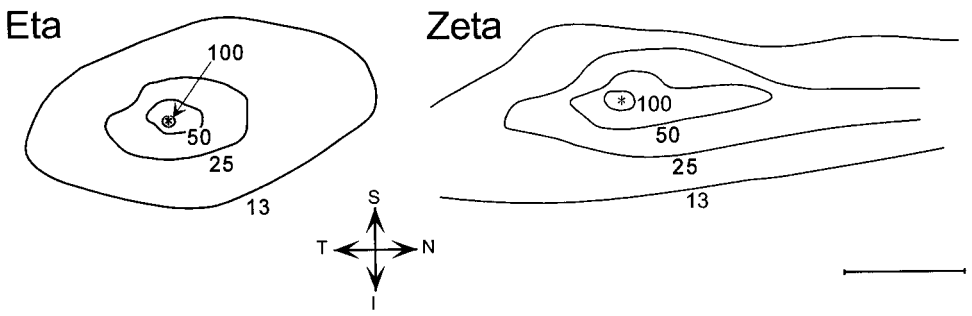

Fig. 12. Comparison of inferred retinal distributions of eta cells (left) and zeta cells (right) of the cat retina. Density estimates obtained for both cell types by assuming a constant dendritic coverage (field area × local density) of 1. Data for zeta cells were reproduced from Berson et al. (1998) with permission from Wiley-Liss, Inc. The asterisk indicates the area centralis, where peak densities reach 146 cells/mm^2 for eta cells and 378 cells/mm^2 for zeta cells. S, superior; I, inferior; N, nasal; T, temporal. Scale bar = 5 mm.

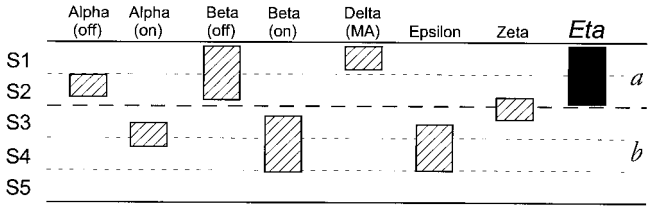

Fig. 13. Schematic summary comparing depth of dendritic stratification of eta cells with those of the other major morphologic ganglion cell types in cat retina. Heavy dashed line marks boundary between sublamina *a* (the OFF sublayer) and sublamina *b* (the ON sublayer) of the inner plexiform layer. MA: monoamine accumulating.

W cells) project ipsilaterally. We note, however, that sample sizes are small and do not exclude participation by eta cells in the crossed temporal projection. The second objection concerns the status of the eta cell as an unpaired morphologic type. Precedents set by the alpha (Y) and beta (X) cells encourage the expectation that functional types sharing most traits but differing in center sign should correspond to a paramorphic pair of anatomic types. OFF-center phasic W cells appear to have ON-center counterparts (Cleland and Levick, 1974a; Stone and Fukuda, 1974), yet eta cells lack a morphologic counterpart ramifying in sublamina *b*. It is possible that the aforementioned expectation is unwarranted. In fact, it has already been contradicted in the case of tonic W (sluggish sustained) cells. Although ostensibly matching ON- and OFF-center varieties of such cells have been identified physiologically (Cleland and Levick, 1974a; Stone and Fukuda, 1974), at least one morphologic counterpart of the ON variety, the epsilon cell, lacks a paramorphic equivalent in sublamina *a* (Pu et al., 1994). Similarly, the monoamine-accumulating delta cell, which appears to correspond to an OFF-tonic W cell, seems to lack a paramorphic counterpart ramifying in sublamina *b* (Dacey, 1989; O'Brien et al., 1999; however, see also Wässle et al., 1987; Wässle and Boycott, 1991). Such failures to observe the expected anatomic pairings suggest a need to reexamine both the concept of paramorphism and the assumption that ON- and OFF-center W cells form functional pairs that match as closely as the ON-X/OFF-X and ON-Y/OFF-Y pairs.

Outputs

Eta cells appear to make a substantial contribution to the retinocollicular pathway. This was expected, because virtually all nonbeta ganglion cells in the cat project to the colliculus (Stein and Berson, 1995). Apparently, eta cells also make a substantial contribution to the retinogeniculate projection. Their projection appears to terminate primarily in the C layers and medial interlaminar nucleus rather than in the A layers and geniculate wing. OFF-center W cells, both phasic and tonic, have been encountered in the C laminae (Cleland et al., 1976; Wilson et al., 1976; Sur and Sherman, 1982), and these are likely to be driven by input from equivalent cell types in the retina, one of which may correspond to the eta cell.

ACKNOWLEDGMENTS

We thank Shane Johnson for his assistance on some of the retrograde tracing experiments, Brian Boycott for his critique of the paper, and Mike Paradiso and Cindi Rittenhouse for donations of cat eyes.

LITERATURE CITED

Amthor FR, Takahashi ES, Oyster CW. 1989a. Morphologies of rabbit retinal ganglion cells with complex receptive fields. J Comp Neurol 280:97–121.

Amthor FR, Takahashi ES, Oyster CW. 1989b. Morphologies of rabbit retinal ganglion cells with concentric receptive fields. J Comp Neurol 280:72–96.

Berson DM, Isayama T, Pu M. 1997. Morphology of presumed ON-OFF direction selective ganglion cell of cat retina. Soc Neurosci Abstr 23:730.

Berson DM, Pu M, Famiglietti EV. 1998. The zeta cell: a new ganglion cell type of the cat retina. J Comp Neurol 399:269–288.

Boycott BB, Wässle H. 1974. The morphological types of ganglion cells of the domestic cat's retina. J Physiol (Lond) 240:397–419.

Chalupa LM, Williams RW, Henderson Z. 1984. Binocular interaction in the fetal cat regulates the size of the ganglion cell population. Neurosci 12:1139–1146.

Cleland BG, Levick WR. 1974a. Brisk and sluggish concentrically organized ganglion cells in the cat's retina. J Physiol (London) 240:421–456.

Cleland BG, Levick WR. 1974b. Properties of rarely encountered types of ganglion cells in the cat's retina and an overall classification. J Physiol (Lond) 240:457–492.

Cleland BG, Levick WR, Morstyn R, Wagner HG. 1976. Lateral geniculate relay of slowly conducting retinal afferents to cat visual cortex. J Physiol (Lond) 255:299–320.

Dacey DM. 1989. Monoamine-accumulating ganglion cell type of the cat's retina. J Comp Neurol 288:59–80.

Dacey DM. 1993a. Morphology of a small-field bistratified ganglion cell type in the macaque and human retina. Vis Neurosci 10:1081–1098.

Dacey DM. 1993b. The mosaic of midget ganglion cells in the human retina. J Neurosci 13:5334–5355.

Dann JF, Buhl EH, Peichl L. 1988. Postnatal dendritic maturation of alpha and beta ganglion cells in cat retina. J Neurosci 8:1485–1499.

Famiglietti EV. 1987. Starburst amacrine cells in cat retina are associated with bistratified, presumed directionally selective, ganglion cells. Brain Res 413:404–408.

Famiglietti EV. 1992. New metrics for analysis of dendritic branching patterns demonstrating similarities and differences in ON and ON-OFF directionally selective retinal ganglion cells. J Comp Neurol 324:295–321.

Famiglietti EV, Kolb H. 1976. Structural basis for 'ON' and 'OFF'-center responses in retinal ganglion cells. Science 194:193–195.

Fukuda Y, Stone J. 1974. Retinal distribution and central projections of Y-, X-, and W-cells of the cat's retina. J Neurophysiol 37:749–772.

Fukuda Y, Hsiao C-F, Watanabe M, Ito H. 1984. Morphological correlates of physiologically identified Y-, X-, and W-cells in the cat retina. J Neurophysiol 52:999–1013.

Hughes A. 1977. Topography of vision in mammals of contrasting life style: comparative optics and retinal organisation. In: Crescitelli F, editor. Visual system in evolution in vertebrates. Handbook of sensory physiology, vol 7, no 5. Berlin: Springer-Verlag. p 613–756.

Isayama T, Berson DM, Pu M. 1997. The theta cell: a bistratified ganglion cell type in cat retina. Invest Ophthalmol Visual Sci 38(Suppl):S51.

Isayama T, O'Brien B, Ugalde I, Frenz A, Aurora V, Tsiaras W, Muller J, Berson D. 1998. Morphology of ferret retinal ganglion cells. Invest Ophthalmol Visual Sci 39:S563.

Kirk DL, Levick WR, Cleland BG. 1976. The crossed or uncrossed destination of axons of sluggish concentric and non-concentric cat retinal ganglion cells, with an overall synthesis of the visual field representation. Vision Res 16:233–236.

Kolb H, Nelson R, Mariani A. 1981. Amacrine cells, bipolar cells and ganglion cells of the cat retina: a Golgi study. Vision Res 21:1081–1114.

Leventhal AG, Keens J, Törk I. 1980. The afferent ganglion cells and cortical projections of the retinal recipient zone (RRZ) of the cat's 'pulvinar complex.' J Comp Neurol 194:535–554.

McGuire BA, Stevens JK, Sterling P. 1986. Microcircuitry of beta ganglion cells in cat retina. J Neurosci 6:907–918.

O'Brien BJ, Isayama T, Berson DM. 1999. Light responses of morphologically identified cat ganglion cells. Invest Ophthalmol Vis Sci (Suppl) (in press).

Peichl L. 1991. Alpha ganglion cells in mammalian retinae: common properties, species differences, and some comments on other ganglion cells. Vis Neurosci 7:155–-169.

Peichl L, Wässle H. 1979. Size, scatter, and coverage of ganglion cell receptive field centers in the cat retina. J Physiol (Lond) 291:117–141.

Pu M, Berson DM. 1991. Morphology of ganglion cells innervating the medial interlaminar nucleus of the lateral geniculate body. Soc Neurosci Abstr 17:709.

Pu M, Berson DM. 1992. A method for reliable and permanent intracellular staining of retinal ganglion cells. J Neurosci Methods 41:45–51.

Pu M, Berson DM, Pan T. 1994. Structure and function of retinal ganglion cells innervating the cat's geniculate wing: an in vitro study. J Neurosci 14:4338–4358.

Ramoa AS, Campbell G, Shatz CJ. 1988 Dendritic growth and remodeling of cat retinal ganglion cells during fetal and postnatal development. J Neurosci 8:4239–4261.

Ramón-Moliner E. 1962. An attempt at classifying nerve cells on the basis of their dendritic patterns. J Comp Neurol 119:211–227.

Rodieck RW. 1998. The first steps in seeing. Sunderland, MA: Sinauer Associates.

Rodieck RW, Brening RK. 1983. Retinal ganglion cells: properties, types, genera, pathways and trans-species comparisons. Brain Behav Evol 23:121–164.

Rodieck RW, Watanabe M. 1993. Survey of the morphology of macaque retinal ganglion cells that project to the pretectum, superior colliculus, and parivcellular laminae of the lateral geniculate nucleus. J Comp Neurol 338:289–303.

Rowe MH, Palmer LA. 1995. Spatio-temporal receptive-field structure of phasic W cells in the cat retina. Vis Neurosci 12:117–139.

Rowe MH, Stone J. 1976. Properties of ganglion cells in the visual streak of the cat's retina. J Comp Neurol 169:99–126.

Rowe MH, Stone J. 1977. Naming of neurons: classification and naming of cat retinal ganglion cells. Brain Behav Evol 14:185–216.

Saito AH. 1983. Morphology of physiologically identified X-, Y-, and W-type retinal ganglion cells of the cat. J Comp Neurol 221:279–288.

Stanford LR. 1987. W-cells in the cat retina: correlated morphological and physiological evidence for two distinct classes. J Neurophysiol 57:218–244.

Stein JJ, Berson DM. 1995. On the distribution of gamma cells in the cat retina. Vis Neurosci 12:687–700.

Stein JJ, Johnson SA, Berson DM. 1996. Distribution and coverage of beta cells in the cat retina. J Comp Neurol 372:597–617.

Stone J. 1983. Parallel processing in the visual system: the classification of retinal ganglion cells and its impact on the neurobiology of vision. New York: Plenum.

Stone J, Clarke RM. 1980. Correlation between soma size and dendritic morphology in cat retinal ganglion cells: evidence of further variation in the gamma-cell class. J Comp Neurol 192:211–218.

Stone J, Fukuda Y. 1974. Properties of cat retinal ganglion cells: a comparison of W-cells with X- and Y-cells. J Neurophysiol 37:722–748.

Sur M, Sherman SM. 1982. Linear and non-linear W-cells in C-laminae of the cat's lateral geniculate nucleus. J Neurophysiol 47:869–884.

Tootle JS. 1993. Early postnatal development of visual function in ganglion cells of the cat retina. J Neurophysiol 69:1645–1660.

Troy JB, Einstein G, Schuurmans RP, Robson JG, Enroth-Cugell C. 1989. Responses to sinusoidal gratings of two types of very nonlinear retinal ganglion cells of cat. Vis Neurosci 3:213–223.

Vaney DI. 1994. Territorial organization of direction-selective ganglion cells in rabbit retina. J Neurosci 14:6301–6316.

Wässle H, Boycott BB. 1991. Functional architecture of the mammalian retina. Physiol Rev 71:447–480.

Wässle H, Levick WR, Cleland BG. 1975. The distribution of the alpha type of ganglion cells in the cat's retina. J Comp Neurol 159:419–438.

Wässle H, Peichl L, Boycott BB. 1981. Morphology and topography of on- and off-alpha cells in the cat retina. Proc R Soc Lond B Biol Sci 212:157–175.

Wässle H, Voigt T, Patel B. 1987. Morphological and immunocytochemical identification of indoleamine-accumulating neurons in the cat retina. J Neurosci 7:1574–1585.

Watanabe M, Rodieck RW. 1989. Parasol and midget ganglion cells of the primate retina. J Comp Neurol 289:434–454.

Watanabe M, Fukuda Y, Hsiao C-F, Ito H. 1985. Electron microscopic analysis of amacrine and bipolar cell inputs on Y-, X- and W-cells in the cat retina. Brain Res 358:229–240.

Weber AJ, McCall MA, Stanford LR. 1991. Synaptic inputs to physiologically identified retinal X-cells in the cat. J Comp Neurol 314:350–366.

Williams RW, Rakic P. 1988. Three-dimensional counting: an accurate and direct method to estimate numbers of cells in sectioned material. J Comp Neurol 278:344–352.

Williams RW, Bastiani MJ, Chalupa LM. 1983. Loss of axons in the cat optic nerve following fetal enucleation: an electron microscopic analysis. J Neurosci 3:133–144.

Wilson PD, Rowe MH, Stone J. 1976. Properties of relay cells in the cat's lateral geniculate nucleus: a comparison of W-cells with X- and Y-cells. J Neurophysiol 39:1193–1209.

Wingate JT, Fitzgibbon T, Thompson ID. 1992. Lucifer yellow, retrograde tracers, and fractal analysis characterise adult ferret retinal ganglion cells. J Comp Neurol 323:449–474.

Wong ROL, Hughes A. 1987. The morphology, number, and distribution of a large population of confirmed displaced amacrine cells in the adult cat retina. J Comp Neurol 255:159–177.